Spatiotemporal patterns of Saharan dust outbreaks in the Mediterranean Basin

György Varga[a*], Gábor Újvári[b] & János Kovács[c,d]

[a]Geographical Institute, Research Centre for Astronomy and Earth Sciences, Hungarian Academy of Sciences, Budaörsi út 45, H-1112 Budapest, Hungary (E-mail: varga.gyorgy@csfk.mta.hu)

[b]Geodetic and Geophysical Institute, Research Centre for Astronomy and Earth Sciences, Hungarian Academy of Sciences, Csatkai E. u. 6-8, H-9400 Sopron, Hungary (E-mail: ujvari@ggki.hu)

[c]Department of Geology & Meteorology, University of Pécs, Ifjúság u. 6, H-7624 Pécs, Hungary (E-mail: jones@gamma.ttk.pte.hu)

[d]Environmental Analytical & Geoanalytical Research Group, Szentágothai Research Centre, University of Pécs, Ifjúság u. 20, H-7624 Pécs, , Hungary

[*]Corresponding author – E-mail: varga.gyorgy@csfk.mta.hu

Abstract

Saharan dust outbreaks transport appreciable amounts of mineral particles into the atmosphere of the Mediterranean Basin. Atmospheric particulates have significant impacts on numerous atmospheric, climatic and biogeochemical processes. The recognition of background drivers, spatial and temporal variations of the amount of Saharan dust particles in the Mediterranean can lead to a better understanding of possible past and future environmental effects of atmospheric dust in the region.

For this study the daily NASA Total Ozone Mapping Spectrometer's and Ozone Monitoring Instrument's aerosol data (1979– 2012) were employed to estimate atmospheric dust amount. Daily geopotential height, wind vector and meridional flow data of the distinguished dust events were obtained from the NCEP/NCAR Reanalysis to compile mean synoptic composite maps. In order to identify the typical dust transportation routes and possible source areas, the backward trajectories were plotted using the NOAA HYSPLIT model.

The main period of the dust transportation is from March to end of August, when the thermal convective activity forces the injection of particles to higher atmospheric levels. However, seasonality patterns of the different Mediterranean sub-basins show quite large differences. In western sub-basins, the maxima of Saharan dust outbreaks is in summer, related southwest flow between a southward emanating trough and the northward migrating subtropical high-pressure centre. In the eastern basin, dust storms occur typically in spring, generated by the warm sector winds on foreside of eastward moving Mediterranean and Sharav cyclones. The seasonal distribution of dust events in the central sub-basins shows a bimodal characteristic with a spring and summer peak.

Highlights:

Saharan mineral dust is an essential component of the Mediterranean atmosphere in spring and summer

The different Mediterranean sub-basins are showing different seasonal aerosol loading patterns and dust transportation pathways

Dust events are connected to different synoptic meteorological situations in the different seasons and sub-basins

Key words: mineral dust; dust storm; Sahara; Mediterranean; synoptic meteorology

Introduction

Atmospheric mineral dust particles are standing in the focal point of recent climatic and various environmental investigations (Stout et al., 2009). Studies of the last two decades recognized and confirmed that mineral dust has significant impacts on numerous atmospheric, climatic and biogeochemical processes (Harrison et al., 2001; Kohfeld and Tegen, 2007; Maher, 2010; Pósfai and Buseck, 2010; Shao et al., 2011). Tropospheric dust particles absorb, scatter and reflect the incoming solar and outgoing terrestrial radiation and modify the albedo of the surface, thereby exerting a direct influence on the energy budget (Arimoto, 2001). By acting as effective cloud condensation nuclei, input of tiny mineral particles into the atmosphere has an effect on life-time of clouds, influencing the radiation balance via an indirect way (Andreae and Rosenfeld, 2008; Klein et al., 2010). However, both direct and indirect effects of atmospheric dust on overall radiation budget remain uncertain, since it depends on its mineralogical, granulometric and related optical properties, atmospheric life-time, concentration and vertical distribution, mostly determined by the chemical composition of source area(s) and by the meteorological background of dust transportation.

Annually, 1–3 billions of tons mineral dust is emitted into the atmosphere from arid-semiarid areas and the most important source regions are situated in Northern Africa; Saharan and Sahel sources are responsible for 50–70% of the global dust emission (Tegen et al., 1996; Mahowald et al., 1999, 2006; Ginoux et al., 2001; Miller et al., 2004). These are unevenly distributed distinct dust hot-spot areas with various seasonal distribution and magnitude of emission, and with different geomorphological characteristics (e.g. ephemeral, salt and dry lakes, ephemeral streams and wadis, seasonal marshes, alluvial fans) (Prospero et al., 2002; Washington et al., 2003; Goudie and Middleton, 2006; Varga, 2012). At these places the

deflation leads to severe soil erosion, loss and coarsening, and also to crop and natural vegetation damage.

Saharan dust can often be observed over the Atlantic Ocean, Mediterranean and Red Sea, and also in the atmosphere of distant areas (e.g. North and South America, Northern Europe). Typically, four main off-coast dust transportation routes can be distinguished: (1) westward transport of the Saharan Air Layer over the North Atlantic (Prospero et al., 1970; Prospero, 1996; Swap et al., 1992); (2) southward to Gulf of Guinea by the Harmattan (McTainsh and Walker 1982); (3) northward to Europe associated with different synoptic meteorological situations (Barkan et al., 2005; Engelstaedter et al., 2006; Stuut et al., 2009; Israelevich et al., 2012; Varga et al., 2013); and (4) eastward to the Middle East (Alpert and Ziv 1989).

The atmosphere of the Mediterranean Basin is highly influenced by dust emission of the surrounding desert areas that release the overwhelming majority of the total Mediterranean aerosols (Moulin et al., 1998; Gkikas et al., 2013). Obviously, the several hundred thousand tons of Saharan dust transported northward influence numerous constituents of environmental systems around the Mediterranean Sea. The increased dust concentration during heavy dust outbreaks often exceed $PM_{2.5}$ and PM_{10} standards of the European Union in Spain (Rodríguez et al., 2001), in Italy (Matassoni et al., 2011) and in Greece (Gerasopoulos et al., 2006), raise the levels of particulate matter in (ambient) air, and hence is able to affect human's health (Griffin et al., 2001; Pey et al., 2012; Morman and Plumlee, 2013). Further, the alkaline dust particles neutralize atmospheric acidity and reduce the frequency of acid rains (Roda et al., 1993, Rogora et al., 2004 and Špoler Čanić et al., 2009).

Iron- and phosphorus-rich particles, acting as fertilizing agents have major impact on marine ecosystems, and through biogeochemical interactions, they affect the primary phytoplankton production and the carbon cycle (Ridgwell, 2002; Maher et al., 2010). Moreover, dust deposited in marine areas could trigger algal blooms (Guerzoni et al., 1999).

Saharan dust addition plays crucial role in the unique Mediterranean terra rossa formation too, where the chemical compounds of soils (e.g. silt sized quartz in limestone or basalt derived soils) can only be explained by some external, aeolian dust accretion as it was identified in Portugal (Jahn et al., 1991), in Spain (Muhs et al., 2010), in Italy (Jackson et al., 1982), in Croatia (Durn et al., 1999), in Greece (MacLeod, 1980), in Turkey (Atalay, 1997) and in Israel (Yaalon and Ganor, 1973; Yaalon, 1997). Small pulses and near-continuous dust addition to soil could affect the whole texture, individual horizons and the fertility by dust-derived nutrients and clay minerals (Simonson, 1995).

Dust activity of Saharan sources has been much more dominant during Pleistocene glacial periods, as it is inferred by the widespread aeolian dust deposits (loess, desert loess, loess-like deposits and marine sediments) of the investigation area with relevant Saharan contribution (Tsoar and Pye, 1987; Cremaschi, 1990; Rózycki, 1991; Hoogakker et al., 2004; Larrasoaña et al., 2008).

For all the mentioned reasons, a better understanding of background drivers of Saharan dust emissions towards the Mediterranean Sea is thought to be a crucial issue. This study is aimed at providing information on the seasonality, synoptic meteorology, transport pathways and source areas of Saharan dust in the atmosphere of different sub-basins of the Mediterranean Sea. In fact, the identification of synoptic meteorological patterns favouring to dust transportation could help to (1) forecast possible severe future dust intrusions; (2) provide analogies for reconstruction of past dusty events; and (3) validate results of global circulation and paleocirculation models.

Methods

For the appropriate monitoring of Saharan dust events, we applied the long-term daily aerosol measurements of NASA's Total Ozone Mapping Spectrometer (TOMS Version8) and Ozone Monitoring Instrument (OMI – Daily Level 3 Gridded Products; OMTO3d) – source: ftp://ftp.toms.gsfc.nasa.gov). The TOMS Aerosol Index (AI) and OMI'S TOMS-like (AI) are measures of how much the wavelength dependence of backscattered ultraviolet radiation from an atmosphere containing aerosols differs from a pure molecular atmosphere, as it was defined by the NASA/GSFC Ozone Processing Team, and given as

$$AI = 100 \times (log_{10} \frac{I_{360meas}}{I_{331meas}} - log_{10} \frac{I_{360calc}}{I_{331calc}}), \quad (1)$$

where I_{360_meas} and I_{331_meas} are the measured 360 nm and 331 nm radiance, and I_{360_calc} and I_{331_calc} are the calculated 360 nm and 331 nm radiance for a Rayleigh atmosphere (Herman et al., 1997; Torres et al., 1998). Positive values of AI indicate absorbing aerosols (dust, smoke from biomass burning), while negative values represent sulphates or sea-salt particles. Since Saharan dust transport into the Mediterranean is generally associated with high aerosol optical depth (Gkikas et al., 2009), higher AI values can rather be explained by dust episodes than sparse biomass burning events. TOMS and OMI TOMS-like AI measurement series were used by several previous studies to identify dust events and source areas (e.g. Prospero et al., 2002; Washington et al., 2003; Gao and Washington, 2009; Varga, 2012).

The sensors have been measuring the atmosphere's absorbing aerosol content since November 1978 on board of different sun-synchronous satellites (1978–1993 Nimbus-7; 1996–2004 Earth Probe; 2005–2012 Aura). As it was showed by Li et al. (2009), that OMI AI is a consistent continuation of TOMS AI of Nimbus-7 and Earth Probe, and according to spatial (Deroubauix et al., 2013) and temporal (Sreekanth and Kulkari, 2013) correlation analyses, and regression analyses with other aerosol products (Ahn et al., 2008), the different AI records can be merged into one aerosol time-series. A 0.75 scale factor was used in the case

of Earth Probe data series, as it was recommended by Hsu et al. (1999). Due to satellite failure (1993–1996) and calibration drift (2001–2004 some measurement series are failed to provide reliable information); even so TOMS and OMI TOMS-like AI has the longest available global record of atmospheric dust emission (Kiss et al., 2007). For the calculations, the 9490 (26×365) daily data-matrices of 1979–1993 (Nimbus-7), 1996–2000 (Earth Probe) and 2005–2012 (Aura OMI) data periods were analysed with MathWorks' MATLAB software, while the average monthly maps were processed in Golden Software SURFER 8. Difference between the resolution of TOMS AI (1°×1.25°) and OMI AI (1°×1°) was handled by kriging interpolation (re-gridding) and by aggregating the gridded data into grid clusters.

The extended investigation area is located between 31°N–43.5°N and 9°W–35°E, sorted into 136 grid clusters for episode identification, time-series and seasonality analyses. Based on the seasonality patterns and geographical distributions, five main Mediterranean sub-basins were distinguished (Fig. 1).

Fig. 1.

We identified days of Saharan dust intrusions by using the standardized AI values ($AI_{st}=(AI-AI_{mean})/\sigma_{AI}$), where AI_{mean} is the yearly regional mean AI, σ_{AI} is the standard deviation and $AI_{st}>1$ values represent a dusty atmosphere (Barkan et al., 2005). In order to define the synoptic meteorological patterns leading to dust intrusion in a given sub-basin, mean geopotential height (700 hPa), wind vector, meridional and zonal flow maps were compiled for the dusty days by using the Daily Mean Composite application of NOAA Earth System Research Laboratory (http://www.esrl.noaa.gov/psd/). According to previous studies, the 700 hPa level represents the average dust transportation altitude (Alpert et al., 2004; Barkan et al., 2005). The centroids of the grid cluster were used as end-points during the 72 h backward-

trajectory analyses, performed by NOAA HYSPLIT (HYbrid Single-Particle Lagrangian Integrated Trajectory) model to determine the main dust transportation pathways (Draxler and Rolph, 2012; Rolph, 2012). The meteorological input for the synoptic calculations and trajectory model was the NCEP/NCAR (National Centers for Environmental Protection/National Center for Atmospheric Research) Reanalysis Project dataset (Kalnay et al., 1996). North Atlantic Oscillation (NAO) Index data were provided by the Climate Analysis Section, NCAR, Boulder, USA, Hurrell (1995).

Results and discussion

General properties of Saharan dust intrusions in the Mediterranean Basin

Mineral particles deflated from Saharan source areas are significant components of the atmosphere of the Mediterranean Sea. However, the frequency and magnitude of dust intrusions show a wide spatial, seasonal and inter-annual variability across the basin. According to our systematic analysis of daily TOMS and TOMS-like AI measurements between 1979 and 2012, Saharan dust could be identified in 23.5% of all measurements in the Western basin (Alboran and Balearic Seas), in 29.5% in the Central Mediterranean (Tyrrhenian and Ionian Seas, Sea of Sicily) and in 33.75% in the Eastern Mediterranean. High amplitude variations determine the annual time series of dusty episodes, with outstanding years of 1984, 1985, 1988, 1999, 2000 and 2008, while the lowest values of annual dust contributions were identified in 1979, 1980, 1981, 1986, 1990 and 2011. The inter-annual (year-to-year) indices of the different sub-basins are correlating well (linear correlation coefficients: Western–Central basins: 0.80; Central–Eastern basins: 0.86; Western–Eastern basins: 0.58). In general, the frequency of dust outbreaks cannot be

unequivocally explained by the changing nature of large scale atmospheric oscillations, circulation patterns or by drought periods.

However, it has previously been documented that during periods of NAO positive phases drier conditions prevail in North-Africa and the frequency of dust outbreaks increase (Cusack et al., 2012; Pey et al., 2013). Pey et al. (2013) have identified a relatively strong correlation between summer North Atlantic Oscillation (NAO) indices and annual Saharan dust contribution to PM_{10} concentration in some parts of the NW Mediterranean (between 2006 and 2011). However, according to our analyses, the relationship of TOMS and OMI AI with both NAO and summer NAO is uncertain for larger areas and for longer periods. Such issues of teleconnections and relationships deserve further investigations in the future.

Atmospheric dust content shows clear seasonal patterns across the different sub-basins (Fig. 2). The main period of Saharan dust intrusions across the Mediterranean is from March to end of August. At these times the atmosphere of North Africa is heavily loaded with dust and the dust outbreaks are primarily determined by synoptic meteorological conditions (Israelevich et al., 2002). The dusty period begins in the early spring in the Eastern Mediterranean and the centres of highest dust concentrations are displaced from east to west from March to September. The AI patterns move back eastwards in September, when dust loadings reduce in the Western basin as a result of the southward migration of the subtropical high pressure belt, while the cyclone activity remain perceptible in the eastern parts. Similar seasonality patterns with March to July maximum in the Eastern Mediterranean and May to August peak in the Central and Western basins were published in several previous studies (e.g. Moulin et al., 1998; Barkan et al., 2005; Israelevich et al., 2012; Pey et al., 2013; Gkikas et al., 2013).

Fig. 2.

The different spatial distribution of the two main seasons of dust contributions could be well identified at meridional transect-analysis plots, where the Aerosol Indices were calculated along 7 vectors for the interval of April and July (two distinct months with intense but spatially diverse dust loading patterns) (Fig. 3). The diagrams clearly demonstrate that at the Eastern basin the April, while at the Western basin the July values are the highest. Dust load into the atmosphere of Central Mediterranean is fairly high in both April and July, so it can be regarded as a transitional area between the two external basins (Pey et al., 2013).

The AI values of the meridional vectors in both cases reflect a decreasing gradient as a function of distance from the African coast. The steeper slope of AI values implies a different kind of dust transportation mechanism and a more evident south-north gradient of intense dust outbreaks. The different seasonal transects are results of the governing different synoptic meteorological situations, which have strong seasonal dependence, as it will discussed in the next section of the paper.

Albeit, the value of AI not only depends on the presence and amount absorbing aerosol particles, but both the transport height and sub-pixel cloud contamination affect it, nevertheless, based on the relatively strong correlation between AI and several other quantitative aerosol products (Kubilay et al., 2005; Kalivitis et al., 2007), we can state that the latitudinal decrease of meridional vectors are primarily governed by the distance from the African coast. A similar, latitudinal gradient decrease was reported by Gkikas et al. (2013).

Fig. 3.

Dust seasonality, synoptic meteorology and transport routes to the different Mediterranean sub-basins

Western Mediterranean (Alboran and Balearic Seas)

At the western part of the Mediterranean Basin (investigation area 1 and 2 – Fig. 1), Saharan dust outbreaks are dominant during the summer months with sporadic dusty episodes in spring. This seasonal distribution pattern is a logical consequence of the synoptic meteorological background of Western Mediterranean dust events as they are controlled by the summer northward migration of the subtropical high-pressure belt. The two separated high cells between 30°N and 35°N, and also a north-south oriented trough can be clearly seen at the mean synoptic map of dust events (Fig. 4). The strong southwestern flow (~10–11 m/s) of dust outbreaks is generated by the steep pressure gradient between the southward emanating deep trough along the western coast of North Africa and the eastern cell of the divided subtropical high-pressure centre over NW Africa. Both the wind flow vectors (at 700 hPa) and backward trajectories (at 3000 m) unambiguously indicate the typical dust transport routes. The highest meridional (southern) wind components (not presented) were identified directly southwest from the investigation areas with an average flow of 8–10 m/s at 700 hPa. At the same time, the zonal (western) wind components are pronounced at the northern fringe of the high-pressure centre.

Fig. 4.

Central Mediterranean (Tyrrhenian and Ionian Seas, Sea of Sicily)

Strong peaks of dust activity in the Central Mediterranean Basin appear in summer with a secondary maximum in spring. As for the region of the Tyrrhenian Sea, Sea of Sicily and Gulf of Gabes (investigation area 4 – Fig. 6) the summer maximum of the bimodal seasonal

distribution curve is more pronounced, compared to the Ionian Sea and Gulf of Sidra domain (area 5 – Fig. 6), where the dust activity is also fairly intense also during the spring. The bimodal seasonality pattern is a result of two predominant synoptic situations. Regarding the springtime dust outbreaks, the main governing atmospheric centre is an eastward moving depression located over the Western Mediterranean and North Africa. Southerly flow is generated by the warm sector winds on foreside of the cyclone. While the strongest meridional flows (~6–7 m/s) at 700 hPa could be identified along the 10°–20°E longitudes, the highest zonal wind components situate over the Sahara between the 20°N and 25°N latitudes.

During the summer dust episodes, the synoptic background resembles that of the previously discussed Western Mediterranean outbreaks. Only a slight difference can be observed in the position of governing pressure centres. The southward emanating deep trough locates nearer to the Atlantic coast of Africa and the high pressure centre situates further east, at ~35°N and ~10°E. Dust laden air-masses are moving at the northern side of this high-pressure centre with a definite zonal (westerly) wind component up to an average speed of 13–14 m/s.

Fig. 5.

Fig. 6.

Eastern Mediterranean

Saharan dust outbreaks are occurring mostly during spring in the Eastern Mediterranean Basin; however, dusty episodes can be observed also in summer, especially in its first half. Eastern Mediterranean dust events are connected to eastward moving atmospheric

depressions. Two different types of low pressure systems can be distinguished in the daily analyses: Sharav cyclones and mid-latitude Mediterranean cyclones (Fig. 7a and 7b). The shallow Sharav cyclones develop at the southern side of the Atlas Mountains as a consequence of steep thermal gradient between the heated continent and the colder sea. Mediterranean cyclones are forming from polar front disturbances enhanced by the complex morphology of the Mediterranean region. Both types of Eastern Mediterranean dust-bearing atmospheric circulations have a fairly strong zonal wind component with a maximum of 12 m/s westerly flow due to their eastward drift. The backward-trajectories clearly demonstrate the predominance of zonal winds over the meridional flows (Fig. 7c).

Fig. 7.

Possible Saharan source areas of Mediterranean dust outbreaks

The appropriate spatial resolution of the TOMS aerosol measurements allows us to identify source areas on regional scale within the major Saharan dust sources, and the detailed analyses of common geomorphological and sedimentary environment of the distinct hot-spots is also possible (Fig. 8). Major sources are associated to specific geomorphological environments. These can be connected to geomorpholocial depressions, ephemeral streams or wadi-systems and to alluvial fans. The fine-grained material of most of the sources was accumulated in some kind of fluvial or lacustrine environment with a certain Pleistocene pluvial history, which acts as a dust source area after the desiccation (Bullard et al., 2008, 2011; McTainsh et al., 2013). Dust transport routes described above enable the more detailed recognition of the most important sources for every Mediterranean sub-basins. The

seasonality patterns of all sources were determined by the analysis of regional time-series data.

Fig. 8.

Activity of dust source areas displays large temporal variability, except for one region, the Bodélé Depression in Chad (marked with (1.1) at Fig. 8.) that is visible all year long and considered as the most active dust source globally. This large depression situates northeast from the Lake Chad, once having been part of the large Lake Mega-Chad (Washington et al., 2006). The fine-grained unconsolidated material of the emissions originates from diatomite deposits of the ancient lakebed, nowadays a series of ephemeral and dry-lakes. Though, the most prominent dust transportation route is from NE to SW towards the Gulf of Guinea (McTainsh and Walker, 1982), in some cases Bodélé can be assumed as the source area of spring outbreaks in the Central Mediterranean Basin (Koltay et al., 2006).

The Azawagh (Azaouak) structural basin is an isolated spot of high dust activity (1.2) framed by the Adrar des Ifoghas, by the Thassili du Hoggar and by the Aïr Mountains. This region was the catchment area of an ancient northern tributary of the Niger River during the Pleistocene pluvial periods (Paris, 1995). The alluvial deposits and the system of ephemeral streams originating from the foothills of Ahaggar (Hoggar) and the Aïr are the sources of the fine-grained loose mineral material.

The remnant of the Pleistocene pluvial lake Araouane in the southern part of the Taoudenni Basin, NW from the large bend of Niger River and west from the Adrar des Ifoghas, is an extensive dust source area (Bridges, 1990). Salt and diatomite deposits of the ancient lakebed can be clearly seen on satellite images and the surface of the enclosed basin is partly covered by extensive system of barchan dunes formed by the prevailing NE trade winds. In fact, the

dust emission mechanism of the region may resemble that of the Bodélé Depression; the bombardment energy of saltating sand particles leads to intensive deflation of the fine-grained particles of lacustrine deposits and enhances dust emission.

At the eastern slopes of gentle hills running parallel to the Atlantic coast a long narrow band of dust sources is located at the western part of the Sahara (1.4). The series of seasonal streams with frequent flash floods in the spring, and sebkhas (e.g. Sebkha Ijil) at the pedimented surface of the Adrar Souttouf and Zemmour Massif bounded by large sand seas, are acting as the main sources of fine-grained material in this region. Mineral deposits of the area are characterised by high illite/kaolinite ratio, high calcite content and are occasionally rich in palygorskite (Scheuvens et al., 2013).

Large alluvial fans and complex wadi-systems at the W and NW slopes of the Ahaggar are acting as an extensive dust source area (1.5). The Tidikelt Depression, at northern part of this region surrounded by plateaus, mountains and by the sand sea of Erg Chech to the west, has an extensive ephemeral drainage system including several wadis from elevated regions, seasonal marshes and mud flats (Glaccum and Prospero, 1980). The heterogeneous mineral composition of source sediments (high kaolinite, sporadic palygorskite and occasionally increased carbonate content) makes it difficult to identify dust storms originated from this region only by their geochemical characteristics.

Clearly, the dust activity of the above discussed regions shows similar variability throughout the year. The atmospheric dust concentration is at a maximum in late spring and summer, and the dust emission of these sources is primary governed by the migration of the Intertropical Convergence Zone (ITCZ) and thermal convective activity of the hottest seasons.

At the southern foreland of the Tell Atlas, a system of salt and dry lakes represents an isolated dust hot-spot area (1.6). Dust emission seems to be largest between Chott Melrhir and Chott Jerid salt lakes, lying north to the Grand Erg Oriental (Prospero et al., 2002). Especially,

Sharav and Mediterranean cyclones transport dust from the zone of chotts (Alpert and Ziv, 1989; Kalderon-Asael et al., 2009). Similar atmospheric circulation patterns are responsible for dust emission from the dusty area expanding from the northern hillslopes of Tibesti through Cyrenaica to the Qattara Depression (1.7) and from the low-lying areas next to the north-south orienting escarpments along the Nile (1.8). For these sources, the main period of dust transportation is in spring with a secondary maximum in summer.

Conclusions/Summary

The regional climatology of TOMS and OMI TOMS-like AI was discussed for the entire Mediterranean region in the period between 1979 and 2012. This study demonstrates that Saharan dust particles are essential components of the Mediterranean atmosphere, especially during spring and summer seasons. This period has been identified as the major interval of high dust loading of the atmoshpere over the Sahara, due to the activity of dust source areas as emitters of wind-blown mineral particles. Obviously, the meteorological factors behind determine the dust transport. Two different types of synoptic situations are associated with Saharan dust outbreaks in the Mediterrranean Basin. During spring mineral particles are carried on the foreside of eastward moving low-pressure systems, responsible for dust events in the Central and Eastern Mediterranean sub-basins. Summer dust episodes are found to be connected to the northward migration of the subtropical high-pressure belt. Regarding the formation of southward moving troughs in the Eastern Atlantic, strong SW flow transports dust towards the Western and Central Mediterranean regions. Depending on the different type of meteorological situations, different areas could serve as dust source regions. As one of the most intense dust source areas, the Bodélé Depression (remnant of ancient Lake Mega-Chad) serves only as occasional source of fine-grained particles of Mediterranean dust outbreaks. At

the same time, the Azawagh structural basin (alluvial deposits and ephemeral streams), the Taoudenni Basin (deposits of Pleistocene Lake Araouane), the Western Saharan sebkhas and ephemeral streams, the Tidikelt Depression, the Ahaggar wadis, Chott Melrhir and Chott Jerid (salt lakes), the extensive wadi-system of Cyrenaica and Qattara Depressions and low-lying areas next to the N-S orienting escarpments along the Nile are identified to be the main source regions of Saharan dust storms delivering high amounts of mineral particles to the Mediterranean Basin.

Acknowledgements

The authors gratefully acknowledge the NOAA Air Resources Laboratory (ARL) for the provision of the HYSPLIT transport model and READY website (http://www.arl.noaa.gov/ready.php) used in this publication. The composite maps of geopotential height and wind vectors were provided by the NOAA/ESRL Physical Sciences Division, Boulder Colorado from their Web site at http://www.esrl.noaa.gov/psd/. Support of the Hungarian Research Fund OTKA under contracts PD108708 (for G. Varga) and PD108639 (for G. Újvári) is also gratefully acknowledged. It was additionally supported by the Bolyai János Research Scholarship of the Hungarian Academy of Sciences and the TÁMOP-4.2.2.C-11/1/KONV-2012-0015 Earth system project for G. Újvári.

References

Ahn, C., Torres, O., Bhartia, P.K., 2008., Comparison of Ozone Monitoring Instrument UV Aerosol Products with Aqua/Moderate Resolution Imaging Spectroradiometer and Multiangle

423 Imaging Spectroradiometer observations in 2006. Journal of Geophysical Research:
424 Atmospheres D16, 27

425 Alpert, P., Ziv, B., 1989. The Sharav Cyclone: Observations and some theoretical
426 considerations. Journal of Geophysical Research 94, 18495–18514.

427 Amante, C., Eakins, B.W., 2009. ETOPO1 1 Arc-Minute Global Relief Model: Procedures,
428 Data Sources and Analysis. NOAA Technical Memorandum NESDIS NGDC 24, 19 p.

429 Andreae, M.O., Rosenfeld, D., 2008. Aerosol–cloud–precipitation interactions. Part 1. The
430 nature and sources of cloud-active aerosols. Earth-Science Reviews 89, 13–41.

431 Arimoto, R., 2001. Eolian dust and climate: relationships to sources, tropospheric chemistry,
432 transport and deposition. Earth-Science Reviews 54, 29–42.

433 Atalay, I., 1997. Red Mediterranean soils in some karstic regions of Taurus mountains,
434 Turkey. Catena 28, 247−260.

435 Barkan, J., Alpert, P., Kutiel, H., Kishcha, P., 2005. Synoptics of dust transportation days
436 from Africa toward Italy and central Europe. Journal of Geophysical Research. Atmospheres
437 110, D07208. 14 p.

438 Barkan, J., Alpert, P., 2010. Synoptic analysis of a rare event of Saharan dust reaching the
439 Arctic region. Weather 65, 208–211.

440 Bridges, E.M., 1990. World Geomorphology. Cambridge University Press, 272 p.

441 Bullard, J.E., Baddock, M., McTainsh, G.H., Leys, J.F., 2008. Sub-basin scale dust source
442 geomorphology detected using MODIS. Geophysical Research Letters 35. L15404. 6 p.

443 Bullard, J.E., Harrison, S.P., Baddock, M.C., Drake, N., Gill, T.E., McTainsh, G., Sun, Y.,
444 2011. Preferential dust sources: a geomorphological classification designed for use in global
445 dust-cycle models. Journal of Geophysical Research 116. F04034 20 p.

446 Cremaschi, M., 1990. Stratigraphy and palaeoenvironmental significance of the loess deposits
447 on Susak Island (Dalmatian archipelago). Quaternary International 5, 97–106.

448 Cusack, M., Alastuey, A., Pérez, N., Pey, J., Querol, X., 2013. Trends of particulate matter
449 (PM2.5) and chemical composition at a regional background site in the Western
450 Mediterranean over the last nine years (2002–2010). Atmospheric Chemistry and Physics 12,
451 8341–8357.

452 Dayan, U., Shoob, T., Enzel, Y., Ziv, B., 2007. Suspended dust over southeastern
453 Mediterranean and its relation to atmospheric circulations. International Journal of
454 Climatology 28, 915–924.

455 Deroubaix, A., Martiny, N., Chiapello, I., Marticorena, B., 2013. Suitability of OMI aerosol
456 index to reflect mineral dust surface conditions: Preliminary application for studying the link
457 with meningitis epidemics in the Sahel. Remote Sensing of Environment 133, 116–127.

458 Draxler, R.R., Rolph, G.D., 2012. HYSPLIT (HYbrid Single-Particle Lagrangian Integrated
459 Trajectory) Model access via NOAA ARL READY Website
460 (http://ready.arl.noaa.gov/HYSPLIT.php). NOAA Air Resources Laboratory, Silver Spring,
461 MD.

462 Durn, G., Ottner, F., Slovenec, D., 1999. Mineralogical and geochemical indicators of the
463 polygenetic nature of terra rossa in Istria, Croatia. Geoderma 91, 125–150.

464 Engelstaedter, S., Tegen, I., Washington, R., 2006. North African dust emissions and
465 transport. – Earth-Science Reviews 79, 73–100.

466 Gao, H., Washington, R., 2009. The spatial and temporal characteristics of TOMS AI over the
467 Tarim Basin, China. Atmospheric Environment 43, 1106–1115.

468 Gerasopoulos, E., Kouvarakis, G., Babasakalis, P., Vrekoussis, M., Putaud, J.P.,
469 Mihalopoulos, N., 2006. Origin and variability of particulate matter (PM10) mass
470 concentrations over the Eastern Mediterranean. Atmospheric Environment 40, 4679–4690.

471 Ginoux, P.M., Chin, I., Tegen, I., Prospero, J., Holben, M., Dubovik, O., Lin, S.J., 2001.
472 Global simulation of dust in the troposhere: model description and assessment. Journal of
473 Geophysical Research 106, 20255−20273.

474 Gkikas, A., Hatzianastassiou, N., Mihalopoulos, N., Katsoulis, V., Kazadzis, S., Pey, J.,
475 Querol, X., Torres, O., 2013. The regime of intense desert dust episodes in the Mediterranean
476 based on contemporary satellite observations and ground measurements. Atmospheric
477 Chemistry and Physics 13, 12135–12154.

478 Glaccum, R.A., Prospero, J.M., 1980. Saharan aerosols over the tropical North Atlantic:
479 mineralogy. Marine Geology 37, 295–321.

480 Goudie, A.S., Middleton, N.J., 2006. Desert Dust in the Global System. Springer, 287 p.

481 Griffin, D.W., Kellogg, C.A., Shinn, E.A., 2001. Dust in the wind: Long range transport of
482 dust in the atmospere and its implications for global public and ecosystem health. Global
483 Change and Human Health 2, 20–33.

484 Guerzoni, S., Chester, R., Dulac, F., Moulin, C., Herut, B., Loye-Pliot, M.D., Measures, C.,
485 Migon, C. Rossini, P., Saydam, C., Soudine, A., Ziveri, P., 1999. The role of atmospheric
486 deposition int he biogeochemistry of the Meditteranean Sea. Progress in Oceanography 44,
487 147–190.

488 Hamonou, E., Chazette, P., Balis, D., Dulac, F., Schneider, X., Galani, E., Ancellet, G.,
489 Papayannis, A., 1999. Characterization of the vertical structure of Saharan dust export to the
490 Mediterranean basin. Journal of Geophysical Research. Atmospheres 104, 22257–22270.

491 Harrison, S.P., Kohfeld, K.E., Roelandt, C., Claquin, T., 2001. The role of dust in climate
492 changes today, at the last glacial maximum and in the future. Earth-Science Reviews 54, 43–
493 80.

494 Herman, J.R., Bhartia, P.K., Torres, O., Hsu, C., Seftor, C., Celarier, E., 1997. Global
495 distribution of UV-absorbing aerosols from Nimbus 7 TOMS data. Journal of Geophysical
496 Research Atmospheres 102, 16911–16922.

497 Hoogakker, B.A.A., Rothwell, R.G., Rohling, E.J., Paterne, M., Stow, D.A.V., Herrle, J.O.,
498 Clayton, T., 2004. Variations in terrigenous dilution in western Mediterranean Sea pelagic
499 sediments in response to climate change during the last glacial cycle. Marine Geology 211,
500 21–43.

501 Hsu, N.C., Herman, J.R., Torres, O., Holben, B.N., Tanre, D., Eck, T.F., Smirnov, A.,
502 Chatenet, B., Lavenu, F., 1999. Comparison of the TOMS aerosol index with Sun-photometer
503 aerosol optical thickness: Results and applications. Journal of Geophysical Research
504 Atmopsheres 104, 6269–6280.

505 Hurrell, J.W., 1995. Decadal Trends in the North Atlantic Oscillation: Regional Temperatures
506 and Precipitation. Science, 676–679.

507 Israelevich, P.L., Levin, Z., Jospeh, J.H., Ganor, E., 2002. Desert aerosol transport in the
508 Mediterranean region inferred from the TOMS aeosol index. Journal of Geophysical
509 Research. Atmospheres 107(D21), 4572, 13 p.

510 Israelevich, P., Ganor, E., Alpert, P., Kishcha, P., Stupp, A., 2012. Predominant transport
511 paths of Saharan dust over the Mediterranean Sea to Europe. Journal of Geophysical Research
512 Atmospheres 117, D02205

513 Jackson, M.L., Clayton, R.N., Violante, A., Violante, P., 1982. Eolian influence on terra rossa
514 soils of Italy traced by quartz oxygen isotopic ratio. In: van Olphen, H., Veniale, F., (eds.):

International Clay Conference, Bologna and Pavia, Italy, September 1981, Elsevier, Amsterdam, 293-300.

Jahn, R., Zarei, M., Stahr, K., 1991. Genetic implications of quartz in “Terra Rossa”-soils in Portugal. Proceedings of 7th Euroclay Conference, Dresden, 541–546.

Kalderon-Asael, B., Erel, Y., Sandler, A. Dayan, U., 2009. Mineralogical and chemical characterization of suspended atmospheric particles over the east Mediterranean based on synoptic-scale circulation patterns. Atmospheric Environment 43, 3963–3970.

Kalivitis, N., Gerasopoulos, E., Vrekoussis, M., Kouvarakis, G., Kubilay, N., Hatzianastassiou, N., Vardavas, I., Mihalopoulos, N., 2007. Dust transport over the eastern Mediterranean derived from Total Ozone Mapping Spectrometer, Aerosol Robotic Network, and surface measurements. Journal of Geophysical Research: Atmospheres 112, D03202

Kalnay, E., Kanamitsu, M., Kistler, R., Collins, W., Deaven, D., Gandin, L., Iredell, M., Saha, S., White, G., Woollen, J., Zhu, Y., Leetmaa, A., Reynolds, B., Chelliah, M., Ebisuzaki, W., Higgins, W., Janowiak, J., Mo, K. C., Ropelewski, C., Wang, J., Jenne, R., Joseph, D., 1996. The NCEP/NCAR 40-Year Reanalysis Project. Bulletin of the American Meteorological Society 77, 437–471.

Kiss, P., Jánosi, I., Torres, O., 2007. Early calibration problems detected in TOMS Earth-Probe aerosol signal. Geophysical Research Letters 34. (7) L07803. 5 p.

Klein, H., Nickovic, S., Haunold, W., Bundke, U., Nillius, B., Ebert, M., Weinbruch, S., Schuetz, L., Levin, Z., Barrie, L.A., Bingemer, H., 2010. Saharan dust and ice nuclei over Central Europe. Atmospheric Chemistry and Physics 10, 10211–10221.

Kohfeld, K.E., Tegen, I., 2007. Record of Mineral Aerosols and Their Role in the Earth System. Treatise on Geochemistry 4, pp. 1–26.

538 Koltay, E., Borbély-Kiss, I., Kertész, Zs., Kiss, Á.Z., Szabó, Gy., 2006. Assignment of
539 Saharan dust sources to episodes in Hungarian atmosphere by PIXE and TOMS observations.
540 Journal of Radioanalytical and Nuclear Chemistry 267, 449–459.

541 Kovács, J., 2008. Grain-size analysis of the Neogene red clay formation in the Pannonian
542 Basin. International Journal of Earth Sciences 97, 171–178.

543 Kubilay, N., Oguz, T., Koçak, M., 2005. Ground-based assessment of Total Ozone Mapping
544 Spectrometer (TOMS) data for dust transport over the northeastern Mediterranean. Global
545 Biogeochemical Cycles 19, GB1022

546 Larrasoaña, J.C., Roberts, A.P., Rohling, E.J., 2008. Magnetic susceptibility of eastern
547 Mediterranean marine sediments as a proxy for Saharan dust supply? Marine Geology 254,
548 224–229.

549 Li, J., Carlson, B.E., Lacis, A.A., 2009. A study on the temporal and spatial variability of
550 absorbing aerosols using Total Ozone Mapping Spectrometer and Ozone Monitoring
551 Instrument Aerosol Index data. Journal of Geophysical Research Atmospheres 114, D09213

552 MacLeod, D.A., 1980. The origin of the red Mediterranean soils in Epirus, Greece. Journal of
553 Soil Science 31, 125–136.

554 Maher, B.A., Prospero, J.M., Mackie, D., Gaiero, D., Hesse, P.P., Balkanski, Y., 2010. Global
555 connenctions between aeolian dust, climate and ocean biogeochemistry at the present day and
556 at the last glacial maximum. Earth-Science Reviews 99, 61–97.

557 Mahowald, N., Kohfeld, K., Hansson, M., Balkanski, Y., Harrison, S.P., Prentice, I.C.,
558 Schulz, M., Rodhe, H., 1999: Dust sources and deposition during the last glacial maximum
559 and current climate: a comparison of model results with paleodata from ice cores and marine
560 sediments. Journal of Geophysical Research 104, 15895−15916.

561 Mahowald, N.M., Muhs, D.R., Levis, S., Rasch, P.J., Yoshioka, M., Zender, C.S., Luo, C.,
562 2006. Change in atmospheric mineral aerosols in response to climate: Last glacial period,
563 preindustrial, modern, and doubled carbon dioxide climates. Journal of Geophysical Research
564 111. D10202. 22 p.

565 Matassoni, L., Pratesi, G., Centioli, D., Cadoni, F., Lucarelli, F., Nava, S., Malesani, P., 2011.
566 Saharan dust contribution to PM10, PM2.5 and PM1 in urban and suburban areas of Rome: A
567 comparison between single-particle SEM-EDS analysis and whole-sample PIXE analysis.
568 Journal of Environmental Monitoring 13, 732–742.

569 McTainsh, G.H., Walker, P.H., 1982. Nature and distribution of Harmattan dust. Zeitschrift
570 für Geomorphologie 26, 417–435.

571 McTainsh G., Livingstone I., Strong C., 2013. Fundamentals of Aeolian Sediment Transport:
572 Aeolian Sediments. In: Shroder, J.F. (ed.) Treatise on Geomorphology, Volume 11, Oxford,
573 Academic Press, 23–42.

574 Middleton, N.J., Goudie, A.S., 2001. Saharan dust: sources and trajectories. Transactions of
575 the Institute of British Geographers NS 26, 165–181.

576 Miller, R.L., Tegen I., Perlwitz, J., 2004. Surface radiative forcing by soil dust aerosols and
577 the hydrologic cycle. Journal of Geophysical Research. Atmospheres 109, D04203, 24 p.

578 Moreno, A., Cacho, I., Canals, M., Prins, M.A., Sánchez-Goñi, M.F., Grimalt, J.O., Weltje,
579 G.J., 2002. Saharan dust transport and high-latitude glacial climatic variability: The Alboran
580 Sea record. Quaternary Research 58, 318–328.

581 Morman, S.A., Plumlee, G.S., 2013. The role of airborne mineral dusts in human disease.
582 Aeolian Research 9, 203–212.

583 Moulin, C., Lambert, C.E., Dayan, U., Masson, V., Ramonet, M., Bousquet, P., Legrand, M.,
584 Balkanski, Y.J., Guelle, W., Marticorena, B., Bergametti, G., Dulac, F., 1998. Satellite

585 climatology of African dust transport in the Mediterranean atmosphere. Journal of
586 Geophysical Research. Atmospheres 103. (D11), 13137–13143.

587 Mounkaila, M., 2006. Spectral and mineralogical properties of potential dust sources on a
588 transect from the Bodélé Depression (Central Sahara) to the Lake Chad in the Sahel.
589 Hohenheimer Bodenkundliche Hefte 78, 1–311.

590 Muhs, D.R., Budahn, J., Avila, A., Skipp, G., Freeman, J., Patterson, DeA., 2010. The role of
591 African dust in the formation of Quaternary soils on Mallorca, Spain and implications for the
592 genesis of Red Mediterranean soils. Quaternary Science Reviews 29, 2518–2543.

593 Paris, F., 1995. Le Bassin de l'Azawagh: pleuplements et civilisations, de néolithique á
594 l'arrivée de l'islam. In: Marliac, A. (ed.) Milieux, sociétés et archéologues, Karthala, 227–
595 260.

596 Pey, J., Querol, X., Alastuey, A., Forastiere, F., Stafoggia, M., 2013. African dust outbreaks
597 over the Mediterranean Basin during 2001–2011: PM10 concentrations, phenomenology and
598 trends, and its relation with synoptic and mesoscale meteorology. Atmospheric Chemistry and
599 Physics 13, 1395–1410.

600 Pósfai, M., Buseck, P.R., 2010. Nature and climate effects of individual tropospheric aerosol
601 particles. Annual Review of Earth and Planetary Sciences 38, 17–43.

602 Prospero, J.M., 1970. Dust in the Caribbean traced to an African dust storm. Earth and
603 Planetary Science Letters 9, 287–293.

604 Prospero, J.M., 1996. Saharan dust transport over the north Atlantic Ocean and
605 Mediterranean: An overview. In: Guerzoni, S., Chester, R. (eds.): The impact of desert dust
606 across the Mediterranean, October 1995, Oristano, Italy, Environmental Science and
607 Technology Library 11, Dordrecht and London: Kluwer, 133–152.

608 Prospero, J.M., Ginoux, P.M., Torres, O., Nicholson, S.E., Gill, T.E., 2002. Environmental
609 characterization of global sources of atmospheric soil dust identified with the Nimbus-7 Total
610 Ozone Mapping Spectrometer (TOMS) absorbing aerosol product. Reviews of Geophysics
611 40, 31 p.

612 Roda, F., Bellot, J., Avila, A., Escarre, A., Pinol, J., Terradas, J., 1993. Saharan dust and the
613 atmospheric inputs of elements and alkalinity to Mediterranean ecosystems. Water, Air, and
614 Soil Pollution 66, 277–288.

615 Rodríguez, S., Querol, X., Alastuey, A., Kallos, G., Kakaliagou, O., 2001. Saharan dust
616 contributions to PM10 and TSP levels in Southern and Eastern Spain. Atmospheric
617 Environment 35, 2433–2447.

618 Rogora, M., Mosello, R., Marchetto, A., 2004. Long-term trends in the chemistry of
619 atmospheric deposition in northwestern Italy: the role of increasing Saharan dust deposition.
620 Tellus B 56, 426–434.

621 Rolph, G.D., 2012. Real-time Environmental Applications and Display sYstem (READY)
622 Website (http://ready.arl.noaa.gov). NOAA Air Resources Laboratory, Silver Spring, MD.

623 Rózycki, S.Z., 1991. Loess and loess-like deposits: evolution of views on the genesis of loess;
624 classical loess provinces; loess of the warm zone. Ossolineum, Wroclaw, 170 p.

625 Scheuvens, D., Schütz, L., Kandler, K., Ebert, M., Weinbruch, S., 2013. Bulk composition of
626 northern African dust and its source sediments – A compilation. Earth-Science Reviews 116,
627 170–164.

628 Shao, Y., Wyrwoll, K.H., Chappell, A., Huang, J., Lin, Z., McTainsh, G.H., Mikami,
629 M.,Tanaka, T.Y., Wangh, X., Yoon, S., 2011. Dust cycle: An emerging core theme in Earth
630 system science. Aeolian Research 2, 181–204.

631 Simonson, R.W., 1995. Airborne dust and its significance to soils. Geoderma 65, 1–43.

632 Špoler Čanić, K., Vidič, S., Klaić, Z.B., 2009. Precipitation chemistry in Croatia during the
633 period 1981–2006. Journal of Environmental Monitoring 11, 839–851.

634 Sreekanth, V., Kulkarni, P., 2013. Spatio-temporal variations in columnar aerosol optical
635 properties over Bay of Bengal: Signatures of elevated dust. Atmospheric Environment 69,
636 249–257.

637 Stout, J.E., Warren, A., Gill, T.E., 2009. Publication trends in aeolian research: an analysis of
638 the Bibliography of Aeolian Research. Geomorphology 105, 6–17.

639 Stöckli, R., Vermote, E., Saleous, N., Simmon, R., Herring, D., 2005. The Blue Marble Next
640 Generation - A true color earth dataset including seasonal dynamics from MODIS. Published
641 by the NASA Earth Observatory.

642 Stuut, J-B.W., Smalley, I., O'Hara-Dhand, K., 2009. Aeolian dust in Europe: African sources
643 and European deposits. Quaternary International 198, 234–245.

644 Swap, R., Garstang, M., Greco, S., Talbot, R., Kallberg, P., 1992. Saharan dust in the Amazon
645 basin. Tellus B 44, 133–149.

646 Tegen, I., Lacis, A.A., Fung, I., 1996. The influence of mineral aerosols from disturbed soils
647 on climate forcing. Nature 380, 419–422.

648 Torres, O., Bhartia, P.K., Herman, J.R., Ahmad, Z., Gleason, J., 1998. Derivation of aerosol
649 properties from a satellite measurements of backscattered ultraviolet radiation: Theoretical
650 basis. Journal of Geophysical Research Atmospheres 103. (D14) 17099–17110.

651 Tsoar, H., Pye, K., 1987. Dust transport and the question of desert loess formation.
652 Sedimentology 34, 134–153.

Újvári, G., Varga, A., Ramos, F.C., Kovács, J., Németh, T., Stevens, T., 2012. Evaluating the use of clay mineralogy, Sr-Nd isotopes and zircon U-Pb ages in tracking dust provenance: an example from loess of the Carpathian Basin. Chemical Geology 304–305, 83–96.

Varga, Gy., 2012 Spatio-temporal distribution of dust storms – a global coverage using NASA Total Ozone Mapping Spectrometer aerosol measurements (1979–2011). Hungarian Geographical Bulletin 61, 275–298.

Varga, Gy., Kovács, J., Újvári, G., 2013 Analysis of Saharan dust intrusions into the Carpathian Basin (Central Europe) over the period of 1979-2011. Global and Planetary Change 100, 333–342.

Washington, R.,Todd, M., Middleton, N.J., Goudie, A.S., 2003. Dust-storm source areas determined by the Total Ozone Monitoring Spectrometer and surface observations. Annals of the Association of American Geographers 93, 297–313.

Yaalon, D.H., 1997: Soils in the Mediterranean region: what makes them different? Catena. 28, 157–169.

Yaalon, D.H., Ganor, E., 1973. The influence of dust on soils during the Quaternary. Soil Science 116, 146–155.

Washington, R., Todd, M., Middleton, N.J., Goudie, A.S., 2003. Dust-storm source areas determined by the total ozone monitoring spectrometer and surface observations. Annals of the Association of American Geographers 93, 297–313.

Wheeler, D.A., 1986. The meteorological background to the fall of Saharan dust, November 1984. Meteorological Magazine 115, 1–9.

Figures

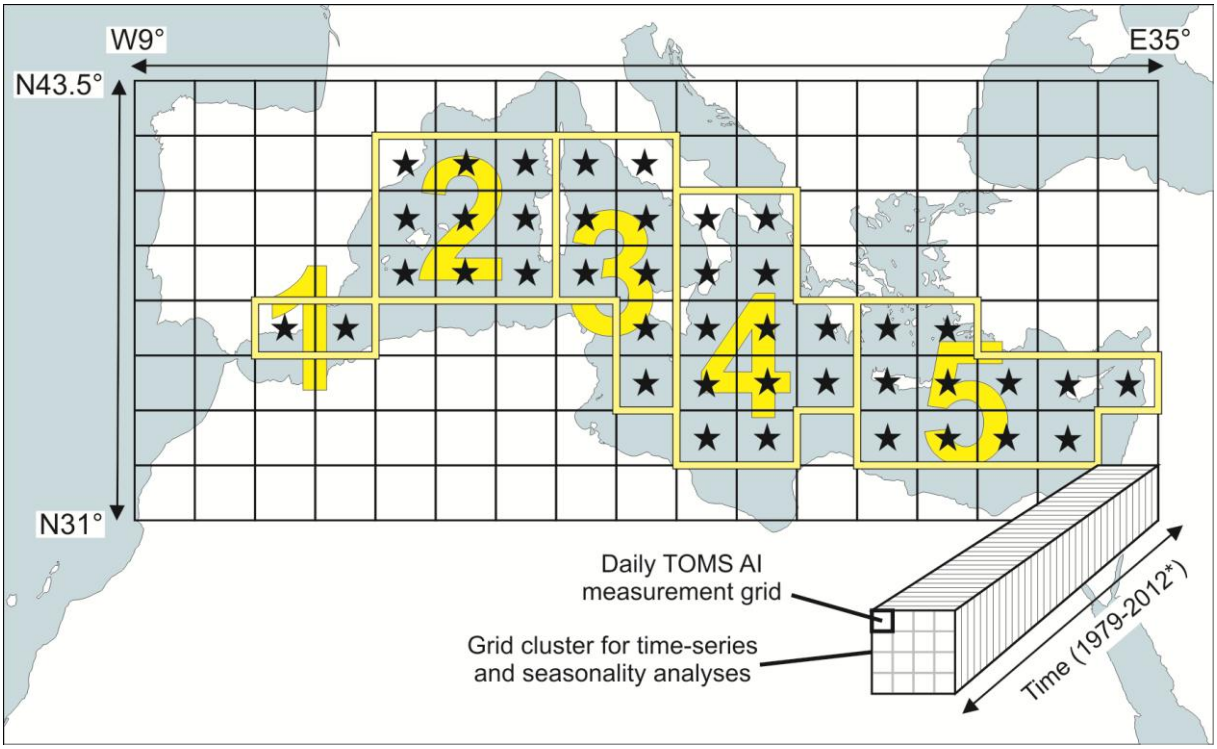

Fig. 1. Schematic map of the investigated area (Black grid clusters have been used for seasonality analyses and black stars denote the centroids of grid clusters for backward-trajectory calculations. Yellow areas indicate the analysed Mediterranean sub-basins.

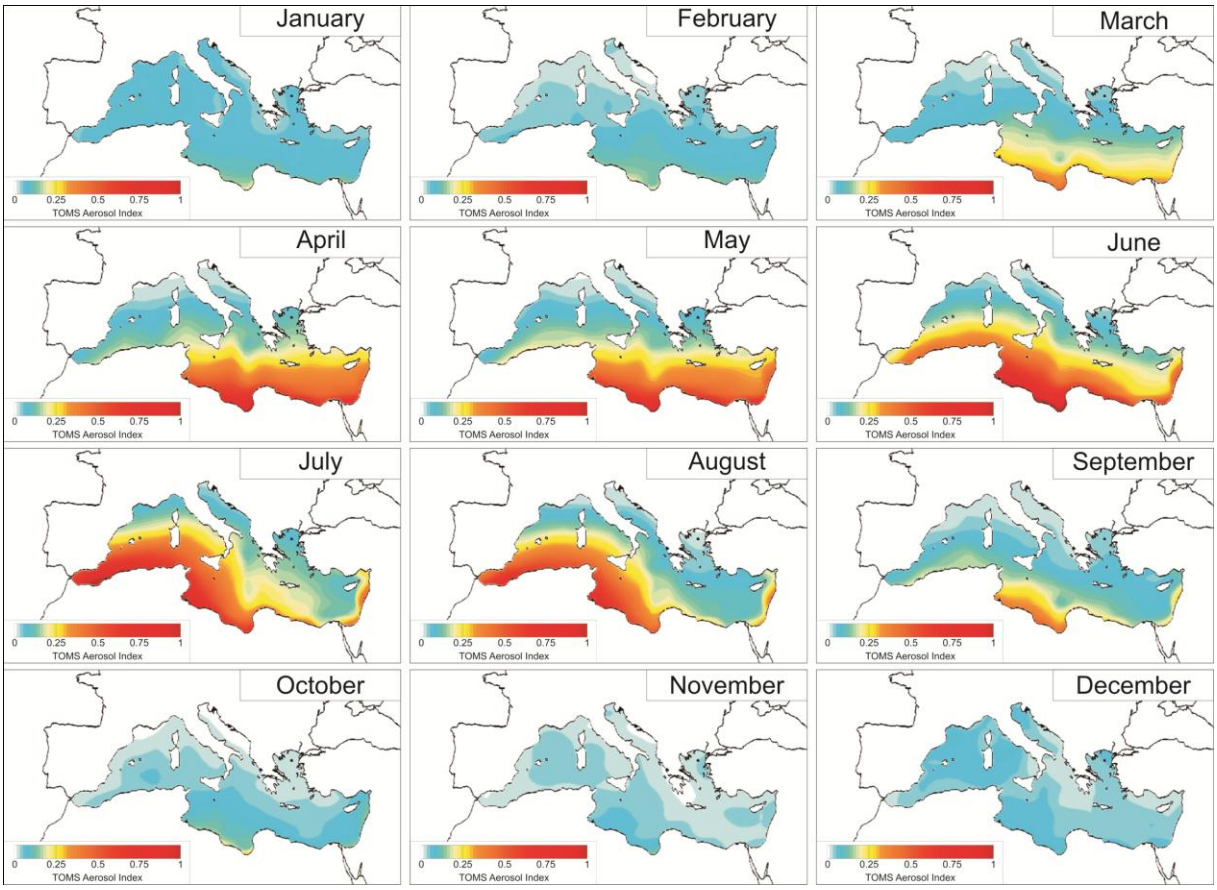

683

684

685 Fig. 2. Monthly mean TOMS aerosol maps of the Mediterranean Sea (1979–2012).

686

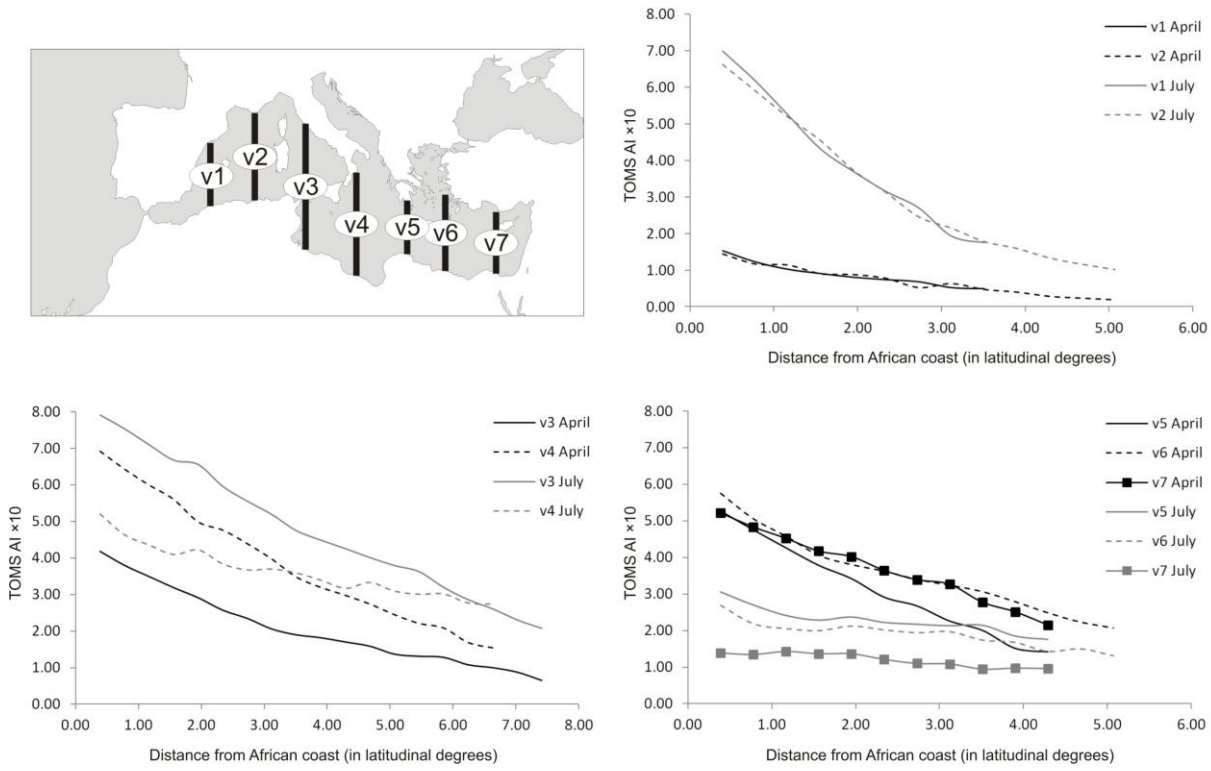

687

688

689 Fig. 3. Meridional transect-analysis of the Mediterranean Basin. TOMS AI values were

690 calculated along the marked 7 vectors.

691

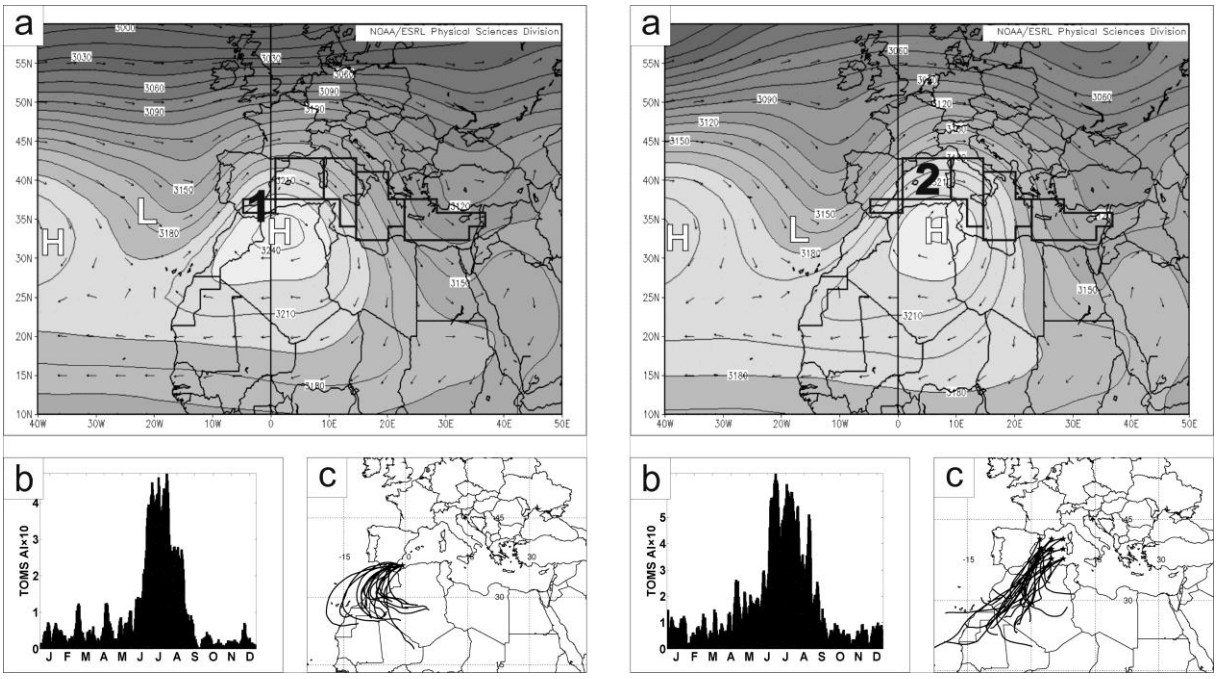

692

693

Fig. 4. General characteristics of Saharan dust intrusions in the Western Mediterranean (sub-basins 1–2): (a) Mean geopotential height and wind vector maps at 700 hPa, (b) seasonal distribution of TOMS AI, (c) typical dust transport routes during the main dust loading period (summer).

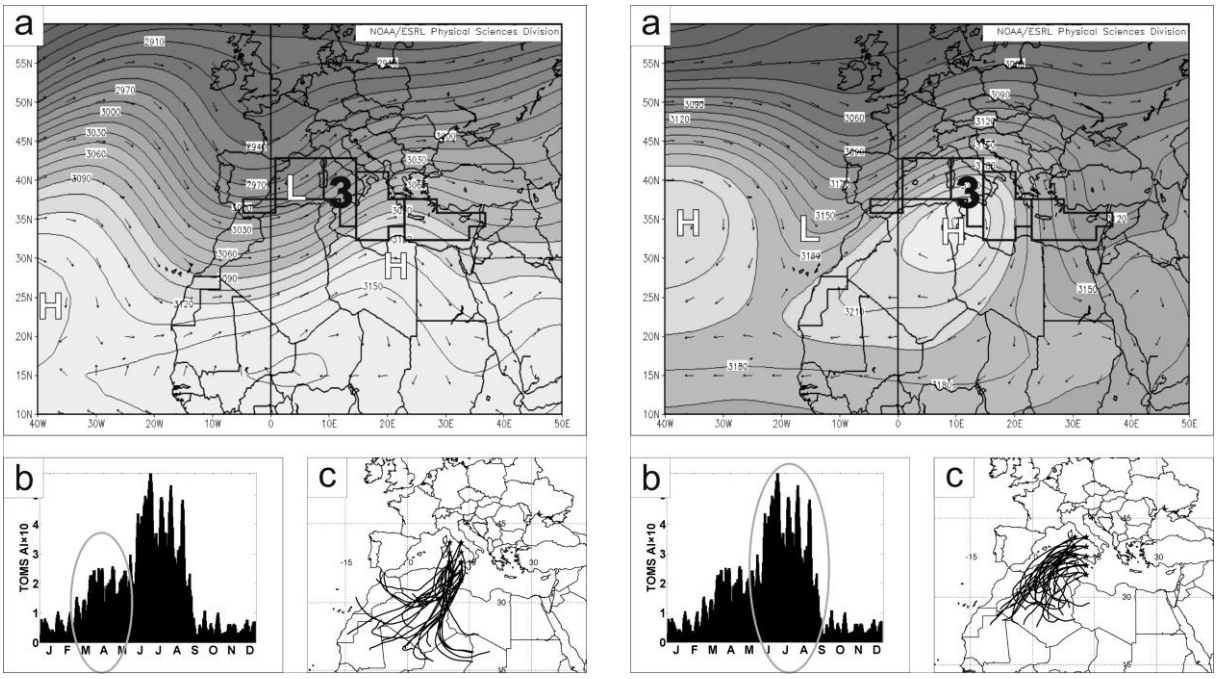

Fig. 5. General characteristics of spring (left) and summer (right) Saharan dust intrusions in the area of Tyrrhenian Sea and Gulf of Gabes: (a) Mean geopotential height and wind vector maps at 700 hPa, (b) seasonal distribution of TOMS AI, (c) typical dust transport routes.

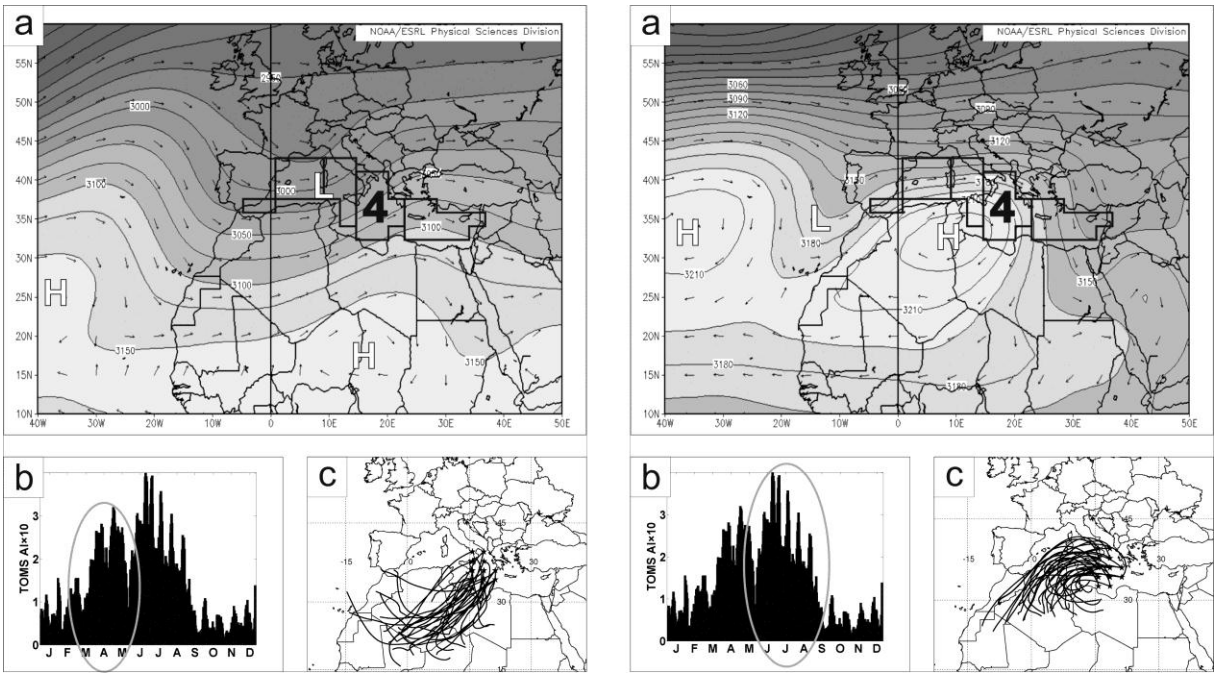

705

706

707 Fig. 6. General characteristics of spring (left) and summer (right) Saharan dust intrusions in

708 the area of Gulf of Sidra and Ionian Sea: (a) Mean geopotential height and wind vector maps

709 at 700 hPa, (b) seasonal distribution of TOMS AI, (c) typical dust transport routes.

710

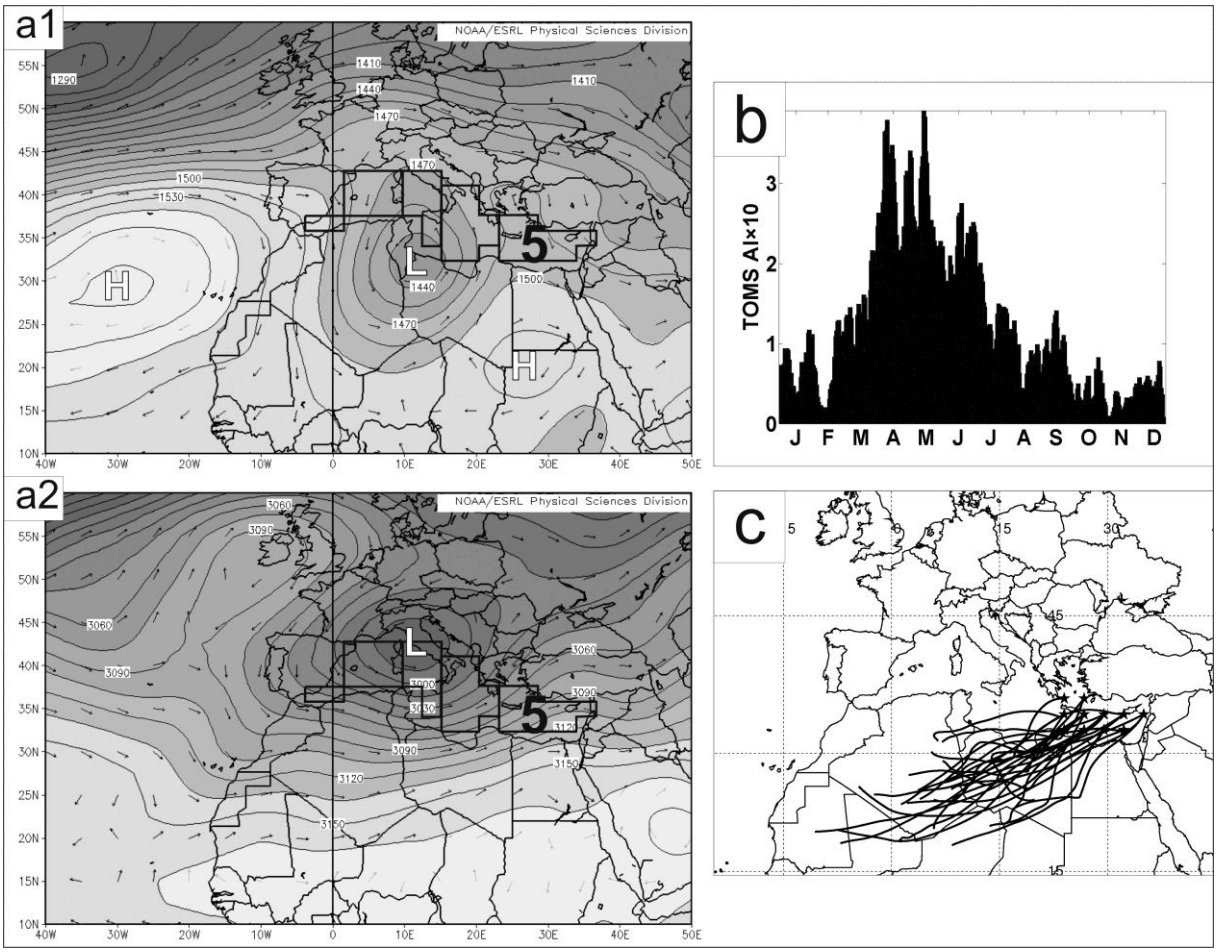

Fig. 7. General characteristics of Saharan dust intrusions in the Eastern Mediterranean: (a1) Mean geopotential height and wind vector maps at 850 hPa of Sharav cyclones, (a2) mean geopotential height and wind vector maps at 700 hPa of Mediterranean cyclones, (b) seasonal distribution of TOMS AI, (c) typical dust transport routes.

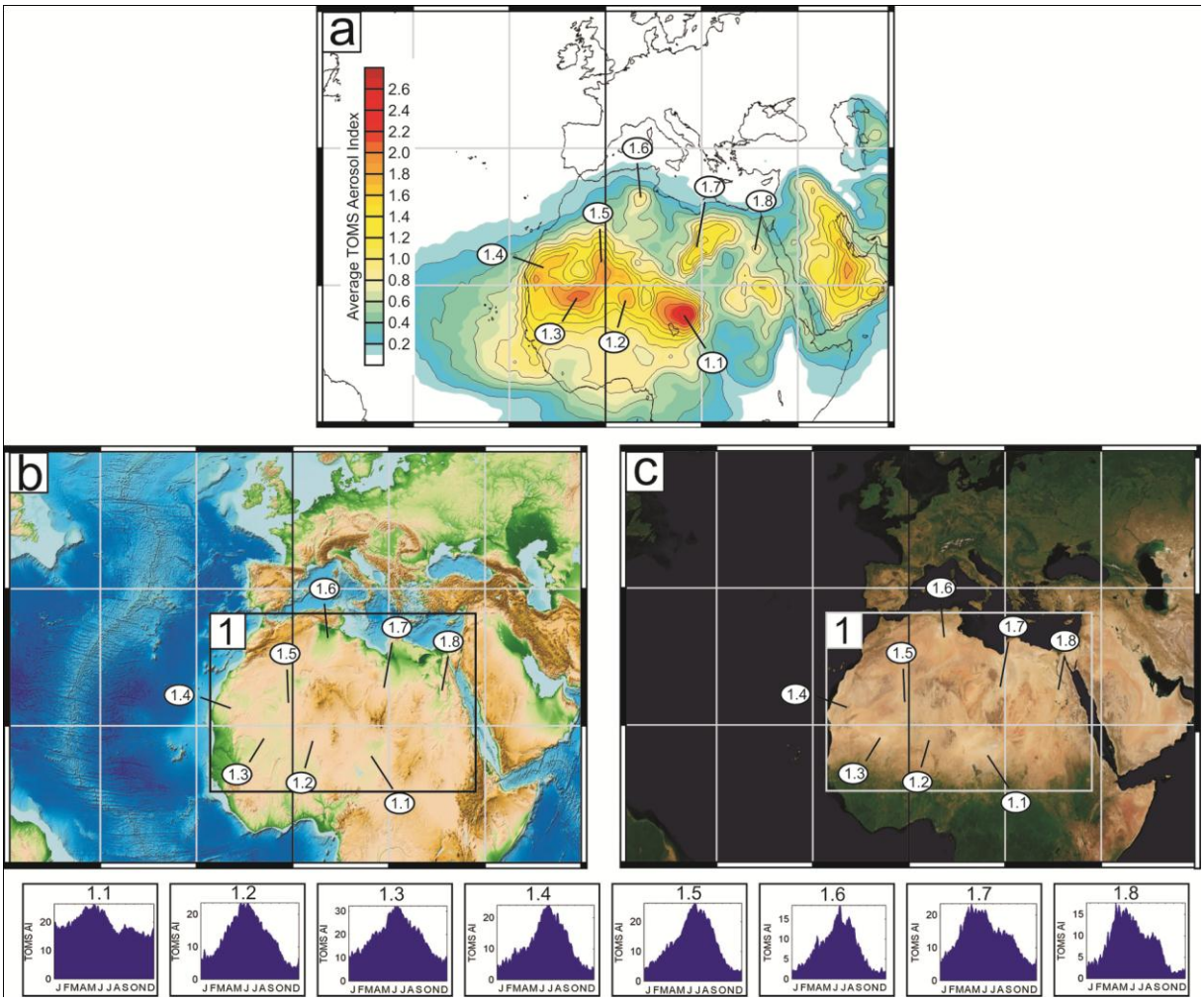

718

719

720 Fig. 8. Geographical distribution and seasonality patterns of major Saharan dust source areas.

721 (a) Average TOMS Aerosol Index map, (b) topographic map – source: Amante and Eakins,

722 2009, (c) NASA Blue Marble Next Generation satellite image – source: Stöckli et al., 2005.